Monolithic Integration of Diffractive Lenses with LED-Arrays for Board-to-Board Free Space Optical Interconnect

Bart Dhoedt, Peter De Dobbelaere, Johan Blondelle, Peter Van Daele, Piet Demeester, *Member, IEEE,* and Roel Baets, *Member, IEEE*

***Abstract*— Since optical interconnections can severely reduce problems associated with electrical interconnect technology (including bandwidth limitations, electromagnetic cross talk, signal delay and EMI aspects), the development of suitable electro-optic components is of crucial importance for implementation of optical interconnects in future computer systems. This paper addresses the design, modeling, fabrication as well as experimental assessment of LED-arrays, with diffractive lenses etched into the rear side of the LED-substrate. The suitability of such optical sources for board-to-board optical interconnections will be demonstrated.**

I. INTRODUCTION

DURING THE PAST few years, several optical interconnection schemes were proposed to replace or supplement existing electrical wiring technology at different interconnect levels (inter cabinet, backplane level, board level, inter chip and even on chip optical interconnects are envisaged). One of the major obstacles for a considerable increase in computer speed is the bandwidth limitation imposed by classical backplane-connector combinations. One possibility to remove this bottleneck is the application of free space line of sight optical data paths (see Fig. 1), facilitating massively parallel communication between adjacent computer boards [1]. Of key importance for the wide scale applicability of this interconnection scheme is the availability at low cost of source and detector arrays. The work described in this paper concentrates on the development of such source arrays, suitable for highly parallel data transmission.

Obviously, arrays of surface emitting laser diodes are quite appropriate for this application. However in this specific situation, being a combination of relatively small (typically 0.25 in) board-to-board spacings (because of requirements on compactness of the resulting computer system) and bandwidths compatible with conventional electronic processing speeds (due to the massively parallel nature of the interconnection, multiplexing several data signals on one physical optical pathway is not necessary, and could even prove disadvantageous in terms of chip cost, electrical routing on the boards, signal delay and reliability), also the option of surface emitting LED-arrays (modulation bandwidth typically limited to 100–200 MHz) seems viable. Moreover, interesting LED-features, including thresholdless operation, low temperature sensitivity, low temporal coherence, lower intrinsic device complexity and hence enhanced component reliability and yield, indicate a substantial advantage of using these components in massively parallel board-to-board applications. It should be noticed that short distance interconnects are preferred for system compactness, making possible the option for LED-arrays as sources.

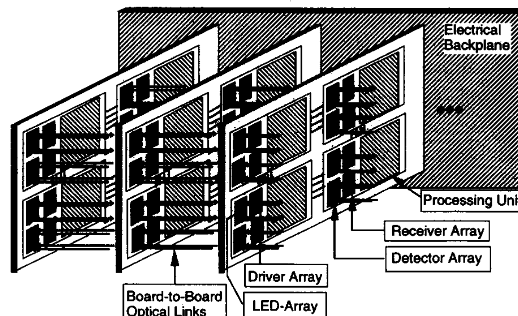

Fig. 1. Free space optical interconnect concept for massively parallel communication between adjacent computer boards.

A major concern in high density arrays of optical beams is related to cross talk avoidance. LED's exhibit a nearly Lambertian radiation pattern, and consequently lens arrays are needed to collimate these beams. Hybrid integration of lenses with LED's (using a solder bump type hybridization process) requires manipulation of individual LED and lens chips. Monolithic integration by etching lenses in the LED-substrate allows wafer scale LED-lens integration, at the expense of additional device processing [2]. In view of its advantage of wafer scale integration of sources with collimating optics, the option for monolithic integration was further explored [3], [4].

Another fundamental choice that has to be made concerns the type of lens to be etched in the component substrate. Obviously, refractive lenses have a strong advantage over diffractive lenses, because the latter tend to spread opti-

Manuscript received May 12, 1994. This work was supported in part by the Commission of the European Union under the ESPRIT III project 6276 HOLICS (Hierarchical Optical Interconnects for Computer Systems) and the Belgian IUAP programme 24 (Inter University Poles of Attraction).
The authors are with the Department of Information Technology (INTEC), University of Gent, Sint-Pietersnieuwstraat 41, B-9000 Gent, Belgium.
IEEE Log Number 9411561.

0733-8724/95$04.00 © 1995 IEEE

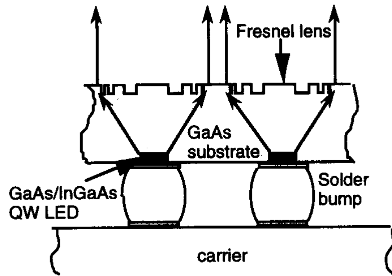

Fig. 2. Schematic component cross section of LED with diffractive lens etched into the substrate.

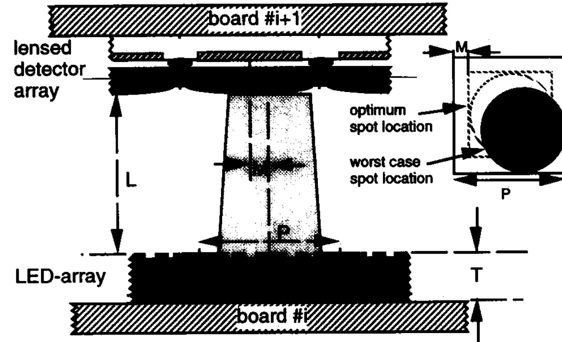

Fig. 3. Geometrical parameters of the parallel free space optical interconnect configuration.

cal power over a number of unwanted diffraction orders, unless a large number of grating levels is used. On the other hand, fabrication of two level diffractive lenses only requires one additional etch step, and is highly reproducible in terms of focusing properties. This argument of relatively low additional device complexity (as compared to conventional LED-sources) led to the option of implementing two level diffractive lenses.

A cross section of the device structure is shown in Fig. 2. Light from the LED's is emitted through the GaAs substrate and is collimated by a two-level diffractive lens. The central wavelength is chosen at 925 nm, assuring sufficient GaAs-transparency and compatibility with Si-photodetectors (limiting the wavelength to 1 μm). The central wavelength of 925 nm can be realized with the GaAs-InGaAs strained layer material system. The component is mounted top down on a carrier (Si or glass) using a solder bump technique [5]. These solder bumps not only assure good mechanical alignment, but also provide electrical access to the individual LED's.

After some design issues, a ray tracing model is presented allowing theoretical performance predictions of the LED-lens combination. Fabrication of the devices is described, paying particular attention to the integration related processing steps. Experimental values for key parameters of the optical interconnect set-up will be given and compared with theoretical results.

II. Component Design

Main parameters of the free space optical interconnect are the array pitch (P), the net free space distance to be covered (L), component substrate thickness (T) and expected level of lateral misalignment (M) (see Fig. 3). Clearly, if cross talk is to be avoided in presence of maximum lateral misalignment, the maximum spot radius in the detector aperture plane (R_I) must obey:

$$2R_I \leq P - 2M. \tag{1}$$

Consider an arbitrary location on the lens surface (distance r_L from the optical axis, see Fig. 4(a) for notations). If rays from all source locations ($0 \leq r_S \leq R_S$), hitting the lens plane at the location should have an Nth diffraction order such that this ray hits the detector aperture plane at $r_I \leq R_I$, we can easily show the local grating period $\Lambda(r_L)$ must satisfy:

$$L(r_L) \leq \frac{N\lambda}{\Lambda(r_L)} \leq U(r_L) \tag{2a}$$

with

$$L(r_L) = n_S \frac{r_L + R_S}{\sqrt{T^2 + (r_L + R_s)^2}} + n_P \frac{r_L - R_I}{\sqrt{L^2 + (r_L - R_I)^2}} \tag{2b}$$

$$U(r_L) = n_S \frac{r_L - R_S}{\sqrt{T^2 + (r_L - R_S)^2}} + n_P \frac{r_L + R_I}{\sqrt{L^2 + (r_L + R_I)^2}} \tag{2c}$$

where

λ: wavelength of incident ray
n_S: substrate refractive index
n_P: propagation medium refractive index.

Relations (2) imply that $L(r_L) \leq U(r_L)$ for all values r_L, being equivalent with:

$$\frac{n_S R_S/T}{\sqrt{1 + (R_S/T)^2}} \leq \frac{n_P R_I/L}{\sqrt{1 + (R_I/L)^2}}. \tag{3}$$

For given values of R_I and L, (3) imposes an upper limit on the R_S/T ratio. Under paraxial conditions ($R_S \ll T, R_I \ll L$), we get $M_L R_S \leq R_I$, with M_L the paraxial lateral magnification. This indicates that the diffractive structure should perform image formation in case the largest allowable source size is chosen. The use of small LED-diameters should be avoided, because of the relatively high current density levels required to obtain a given optical output power, and the reduced quantum efficiency related with nonradiative surface recombinations. Consequently, the substrate thickness T should be chosen as large possible, whilst allowing the use of standard processing equipment.

The use of diffractive optics in combination with optical sources exhibiting relatively large optical bandwidths (typical full width half maximum LED bandwidths are about 5% of the central wavelength for the GaAs/InGaAs material system),

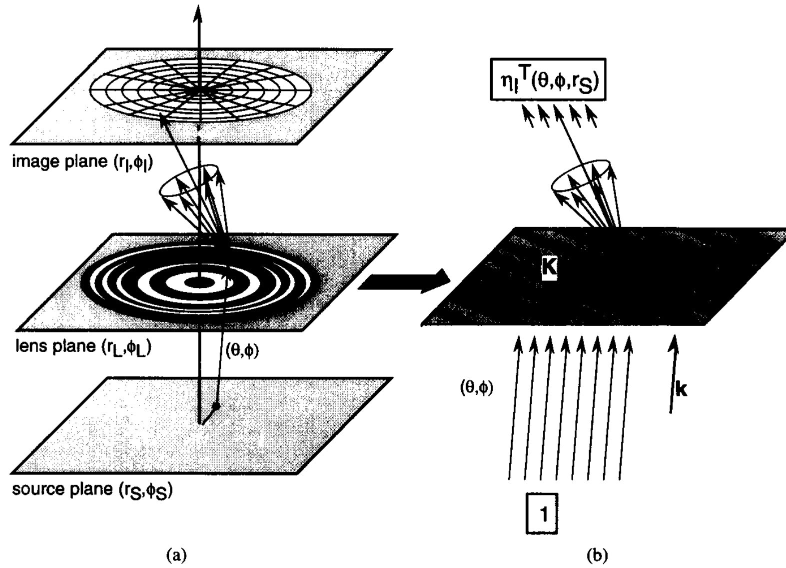

Fig. 4. Ray tracing procedure for derivation of optical power density profiles in arbitrary planes.

implies that condition (2) must hold for a complete wavelength range $[\lambda_c - \Delta\lambda/2, \lambda_c + \Delta\lambda/2]$. Therefore

$$\frac{L(r_L)}{\lambda_c - \Delta\lambda/2} \leq \frac{N}{\Lambda(r_L)} \leq \frac{U(r_L)}{\lambda_c + \Delta\lambda/2}. \quad (4)$$

The largest allowable $\Delta\lambda$ occurs when the under limit in (4) equals the upper limit, and we get

$$\Delta\lambda(r_L) = 2\frac{U(r_L) - L(r_L)}{U(r_L) + L(r_L)}\lambda_c \quad (5)$$

which is clearly a function of lens location. The worst case wavelength range the lens will focus such that $r_I \leq R_I$ is $\Delta\lambda(R_L)$. For locations closer to the optical axis this wavelength range will be larger. The local grating period as a function from r_L is then derived from (2) and (4):

$$\Lambda(r_L) = \frac{2N\lambda_c}{L(r_L) + U(r_L)}. \quad (6)$$

Under paraxial conditions (6) reduces to

$$\Lambda(r_L) = \frac{N\lambda_c f}{r_L} \quad (7)$$

and (5) becomes

$$\Delta\lambda(r_L) = \frac{2\lambda_c f}{r_L}\frac{n_P}{L}(R_I - M_L R_S) \quad (8)$$

indicating that, if the maximum allowable source diameter R_I/M_L is chosen, the configuration only works properly for the central wavelength. Other wavelength components are focused such that $r_I > R_I$, contributing to cross talk. In (7) and (8) f stands for the paraxial focal distance of the lens, i.e.,

$$\frac{1}{f} = \frac{n_S}{T} + \frac{n_P}{L}. \quad (9)$$

It can easily be derived from elementary Fourier optics that $1/2N$ is the optimum grating duty cycle for a two-level binary phase grating for maximum Nth order diffraction efficiency. Technology, and more specifically lithography, however imposes limits on grating features. Let F be the minimum feature size allowable for high yield lens definition and fabrication. The optimum local grating duty cycle, given the constraint on feature sizes, is then

$$d_c(r_L) = \max\left(\frac{F}{\Lambda(r_L)}, \frac{1}{2N}\right). \quad (10)$$

The minimum grating period that can be realized is clearly $\Lambda_m = 2F$. In the central zone of the lens, the optimum duty cycle of $1/2N$ can be implemented. When $\Lambda(r_L)$ reaches $2NF$ the grating fringes remain of fixed width F, while the grating duty cycle increases moving away from its optimum value $1/2N$. When $\Lambda(r_L)$ reaches $2F$ the maximum lens aperture for this diffraction order has been reached. In the paraxial case, the maximum lens aperture for which the duty cycle maintains its optimum value of $1/2N$ is not dependent on the diffraction order used, and is given by

$$A = \frac{\lambda_c f}{2F}. \quad (11)$$

The total lens radius, i.e., including a nonoptimum duty cycle zone, amounts to NA. As the grating duty cycle moves farther away from its optimum value, the optical power coupled to unwanted diffraction orders increases. Therefore, in cross talk limited situations, the lens aperture should be reduced at the expense of inferior optical power transfer.

Because diffraction efficiencies decrease for higher orders, one should use first order diffraction wherever possible. On the other hand, use of Nth order diffraction gives, according to (6) local grating periods N times larger than first order grating periods, allowing larger lens apertures. Consequently,

TABLE I
FREE SPACE INTERCONNECTION CONFIGURATION

free space interconnect distance		L	μm	2600.0
lateral misalignment design goal		M	μm	50.0
substrate thickness		T	μm	500.0
array pitch		P	μm	500.0
minimum feature size		F	μm	1.0
substrate refractive index		n_S		3.5
propagation medium refractive index		n_P		1.0
central optical wavelength		λ_c	nm	925
maximum spot radius in detector plane	(1)	R_I	μm	200.0
maximum source radius	(3)	R_S	μm	11.0
paraxial lens focal distance	(9)	f	μm	135.4
paraxial lateral magnification		M_L		18.2
radius of optimum duty cycle zone	(11)	A	μm	62.6

the optimum lens design will use first order diffraction in the central zone and second order diffraction in the periphery. Again, if the interconnect is limited by cross talk rather than power transfer, use of this second order zone might be disadvantageous.

The hybrid lens we end up with can be seen as a combination of two diffractive lenses with a different primary focus. The first order lens (primary focus at f), has higher order foci at $f/2, f/3 \cdots$. The second order lens (primary focal distance $2f$) has higher order foci at $f, 2f/3, f/2, \cdots$. The combination of the two lenses exhibits a large number of foci, including a common focal point at f.

The radii of the grating fringes can be derived by imposing relation (6) in the middle of each grating "period." Suppose the mth grating radius is known (r_m), and values r_{m+1} and r_{m+2} are sought. The local grating period is $r_{m+2} - r_m$. Applying (6) in the middle of this period yields:

$$r_{m+2} - r_m = \Lambda\left(\frac{r_{m+2} + r_m}{2}\right) \tag{12a}$$

which can be solved for r_{m+2}. The value of r_{m+1} is then easily found from the grating duty cycle (9):

$$r_{m+2} - r_{m+1} = d_c\Lambda\left(\frac{r_{m+2} + r_m}{2}\right). \tag{12b}$$

Starting from the requirement that diffracted rays of a certain order should be focused within a well defined area in the detector aperture plane, expressions for local grating period, optical wavelength range as well as for the grating fringes radii have been derived leading to a lens design strategy for maximum optical power throughput. These principles will be applied to the configuration given in Table I.

Fig. 5 shows curves of $\Delta\lambda$ (5) against lens aperture for a number of source sizes, which is, as already stated, a pessimistic estimate for the wavelength range where the diffractive structure correctly focuses. If optical bandwidths of ca. 50 nm are expected, Fig. 5 suggests that lenses with aperture $A = 62.6$ μm (Table I) imply $R_S \leq 10.0$ μm. Lenses having an aperture twice as large require $R_S \leq 7.5$ μm. Introducing values from Table I in (8), together with $\Delta\lambda = 50$ nm gives $R_S \leq 9.2$ μm for a lens with aperture A and $R_S \leq 7.4$ μm for a 2 A aperture lens.

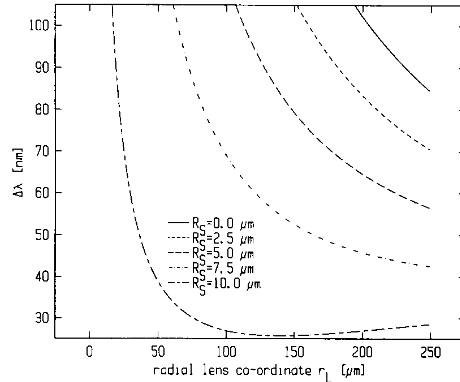

Fig. 5. Wavelength range where the lens correctly focuses as a function of lens radial co-ordinate r_L for a number of source radii R_S.

TABLE II
PROPERTIES OF IMPLEMENTED LENSES

	purely first order lens	combined lens
focal distance	f=135.4 μm	f=135.4 μm
lens structure	• first order diffraction • duty cycle : 50 % • aperture = A = 62.5 μm • minimum feature : 1 μm	• central zone : - first order diffraction - duty cycle 50 % • periphery : - second order diffraction - duty cycle varying from 25 % to 50 % • aperture = 2A = 125 μm • minimum feature : 1 μm
performance • cross talk • power throughput	 low cross talk reduced power transfer	 high cross talk higher power transfer

For the interconnect configuration shown in Table I, a mask set was developed. In order to be able to trade off properties (relating to power throughput and cross talk), two lens types were implemented (Table II), both with minimum feature size 1 μm. This minimum feature size is compatible with widely available photolithography equipment and fabrication processes. Mesa diameters on the masks should not be chosen too close to the limits given above, because current spreading tends to extend the light emitting region beyond the mesa area. On the other hand, small mesas are disadvantageous in terms of quantum efficiency and lifetime (larger current densities for a fixed optical output power level). Two mesa sizes were implemented on the mask: $R_S = 6\,\mu$m and $R_S = 8\,\mu$m.

III. DIFFRACTION MODEL

This section describes a ray-tracing based diffraction model, which will be used to predict the focusing properties of the LED-lens device. Because of the large refractive index contrast, occurrence of grating features with sizes comparable with the wavelength and oblique incidence, diffraction models based on transmission functions become inaccurate [6]. Rigorous modeling of the complete lens structure seems unpractical because of its size [7] (the diameter of the large aperture lens amounts to 270 λ), and would require huge computer hardware resources.

To find a good compromise between full rigorous electromagnetic modeling of the complete lens structure and the inaccurate, but straightforward transmission function approach, a ray tracing based model was developed, which

is expected to yield good results in the case of incoherent sources. This ray tracing procedure is based on breaking up the diffractive structure in small substructures, which are assumed to be perfectly periodical. These periodic structures are then treated by a rigorous diffraction model. The algorithm consists of the following steps (see Fig. 4), eventually leading to optical power densities in an arbitrary plane behind the diffractive lens:

1) The circular source is decomposed in a set of point sources (co-ordinates (r_S, ϕ_S) of equal intensity.
2) For each point source, a set of rays (θ, ϕ) is traced through the structure, carrying an equal optical power when emitted by the source.
3) For each ray, following quantities are determined:
   a) position of incidence in the lens plane (r_L, ϕ_L)
   b) local grating period $\Lambda(r_L)$
   c) propagation vectors of forward diffracted rays
   d) diffraction efficiency of each transmitted order
   e) location of beam incidence in the image plane (r_I, ϕ_I) for each diffracted order
4) A grid is constructed in the image plane, and the optical power density in each grid cell is found by summing all contributions from all diffracted rays.

Optical power density in cell (i, j) comprised within boundaries $[R_{1i}, R_{2i}]$ and $[\phi_{1j}, \phi_{2j}]$ is then given by

$$P_{ij} = \frac{1}{2} \int_0^{R_S} r_S \frac{dr_S}{\pi R_S^2} \int_0^{2\pi} \frac{d\phi}{2\pi} \int_0^{\pi/2} \sin\theta \, d\theta \cdot \sum_{\substack{\text{propagating} \\ \text{orders } l}} \eta_l^T(\theta, \phi, r_S) w_{ij}(r_{Il}, \phi_{Il}) \quad (13)$$

with

$$w_{ij}(r, \phi) = \begin{cases} 1, & R_{1i} \le r \le R_{2i} \text{ and } \phi_{1j} \le \phi \le \phi_{2j} \\ 0, & \text{else} \end{cases}$$

$\eta_l^T(\theta, \phi, r_S)$: order l transmitted diffraction efficiency, for ray emitted by a source at r_S in direction determined by angles (θ, ϕ)

$(r_{Il}(\theta, \phi, r_S), \phi_{Il}(\theta, \phi, r_S))$: (r, ϕ) co-ordinates in the image plane of the location of incidence of order l diffracted ray, originating from a ray emitted by a source at r_S and emission angles (θ, ϕ).

Due to the symmetry of geometry and excitation, integration over angle ϕ_S is not necessary. Optical power density in the image plane is normalized to 0.5 (half of the power is lost by rays emitted in the wrong direction, i.e., $-\pi/2 \le \theta \le 0$). In reality, some of this optical power is recuperated by reflection on the metallic contact layer.

The only remaining problem remains the computation of the diffraction efficiencies $\eta_l^T(\theta, \phi, r_S)$. These values are obtained by solving an associated, but far less complicated, grating diffraction problem (Fig. 4): a plane wave with same $\boldsymbol{k}$-propagation vector as the ray is incident upon a grating with period $\Lambda(r_L)$. The grating $\boldsymbol{K}$-vector is oriented perpendicular to the circular fringes of the original diffractive lens, giving raise to a three-dimensional conical diffraction problem. Rigorous solution of this electromagnetic problem using a coupled wave formalism is treated in [8], [9].

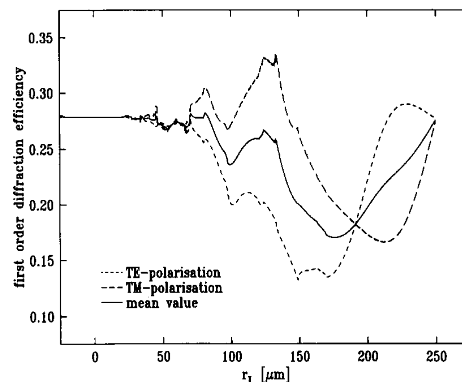

Fig. 6. First order diffraction efficiencies for a purely first order lens as a function of radial co-ordinate in the lens plane r_L (on axis point source, $\lambda = 925$ nm).

First order diffraction efficiencies for a purely first order lens (focal distance in air $f = 135.4\,\mu$m) are shown in Fig. 6 as a function of radial co-ordinate in the lens plane r_L for an on axis point source ($\lambda = 925$ nm). No limitations on minimum feature size were imposed. Etch depth was set to 180 nm (π phase shift for $\Delta n = 2.5$ at 925 nm) and grating duty cycle was chosen 50%. Interesting to notice is that for $r_L \ge 150\,\mu$m (substrate thickness 500 μm), the critical angle for a GaAs-air interface is reached, but nevertheless a considerable amount of optical power is transmitted through first order diffraction.

Fig. 7 gives for the same $f = 135.4$ μm lens the total optical power in focused diffraction orders for the two lens types discussed in Section II. Optical powers, relative to a total emitted power of 1, are given as a function of the mask minimum feature size F. Since the LED-pitch is 500 μm, the lens radius is limited to 250 μm. For the first order lens this aperture is reached for $F = 0.27$ μm, while the combined lens fills the full aperture available at $F = 0.55$ μm. Consequently, power throughput remains constant for $F \le 0.27$ μm and exhibits a kink at $F = 0.55$ μm in the large aperture lens case. Performance difference between the two lens types is most pronounced for this F-value. For $F = 1$ μm, we get 0.14 and 0.19% for the small aperture and large aperture lenses, respectively, or a relative increase in power transfer of 33%.

Expected power density profiles along the radial co-ordinate in the image plane r_I are represented in Fig. 8 in the $R_S = 6$ μm case for a number of propagation distances L. It can be seen from these figures that spot sizes are for both lenses (described in Section II) compatible with the 200 μm spot radius design goal.

IV. Fabrication Issues

As mentioned above, the requirements of GaAs substrate transparency and compatibility with Si photo detectors led to a central wavelength setting of 925 nm, suggesting the GaAs-InGaAs strained layer material system. Because LED-diameters are fairly small, three quantum wells (4.4 nm $In_{17}Ga_{83}As$) were incorporated in the LED active layer to prevent saturation of optical output power at low current levels.

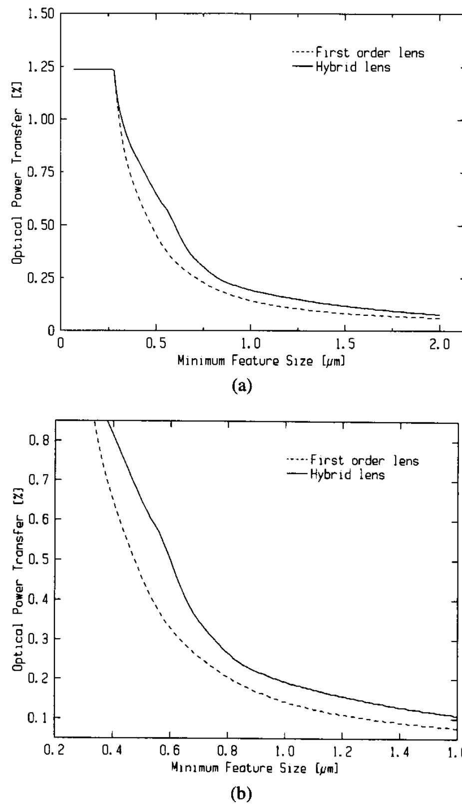

Fig. 7. Total optical power in focused diffraction orders for the lenses of Table II as a function of minimum feature size F. Graph (b) contains the same information as (a), but on a different scale.

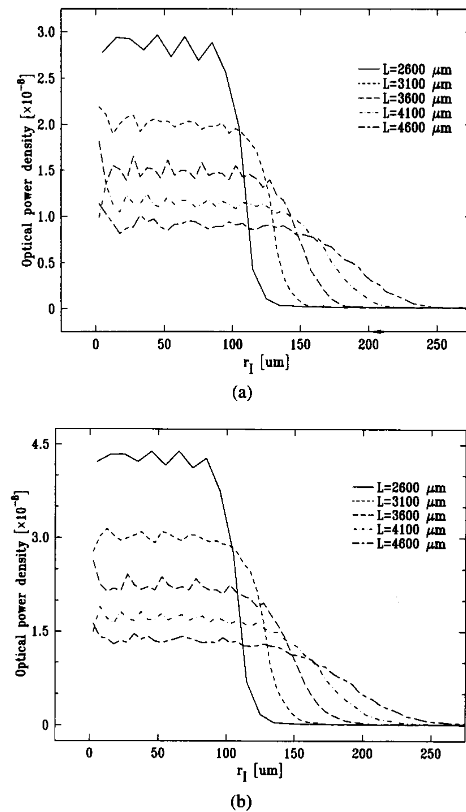

Fig. 8. Modeled power density profiles for different propagation distances L. Data is for the $R_S = 6\ \mu$m} source, (a) first order lens, (b) combined lens.

In order to optimize light emission from the active layer, a GRIN structure (thickness 200 nm) was grown at both sides of the active layer.

Because etching of the Fresnel lens is a nonconventional processing step, and therefore considered risky to perform on fully processed LED-devices, definition of the diffractive structure was done immediately after the MOCVD growth of the epitaxial layer structure. To protect the layer structure during the lens etching process, a SiO_x layer was deposited by PE-CVD. After conventional contact photolithography, the lenses were etched by $SiCl_4$ based reactive ion etching (RIE) (Fig. 9). Groove depth was aimed at 180 nm, and it was shown that after one etching rate calibration step (yielding groove depth 135 nm), this value can be reached within 10 nm accuracy. A protective poly-imide layer was spun on the lens side to prevent damage to the diffractive structures during processing of the mesa side.

After removal of the SiO_x protective layer, lithography for the mesas was performed. This was done by through substrate IR-illumination. Misalignments at this level would result in obliqueness of the output beam, making this difficult alignment step crucial for the proper operation of the device. As will be shown in the measurement section, alignment accuracy of the mesa's with respect to diffractive lenses is in the 1 μm range.

Fig. 9. SEM-photograph of large aperture diffractive lens (diameter 250 μm). Smallest features are 1 μm.

The LED structure is then realized by conventional processing steps, comprising deposition and etching of isolation layer (SiO_x), evaporation of p-contact metallization layer (Ti/Au), deposition of a second isolation layer (SiO_x) defining wettable pads. On the mesa side again a protective poly-imide layer was spun, and the n-contact metallization (AuGe/Ni) was deposited and etched, leaving apertures for the diffractive lenses. Both sides are then gold plated (after protective layer removal at mesa side) to improve bonding properties.

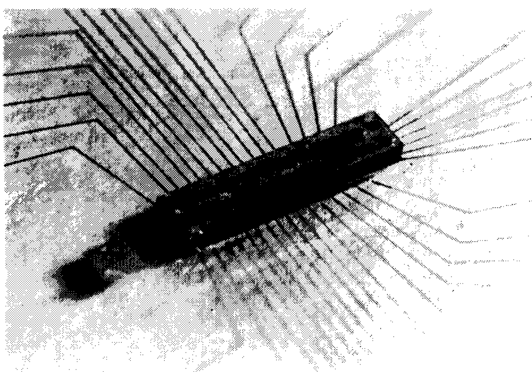

Fig. 10. Flip chip mounted LED-array on glass carrier. One array contains 36 LED's, and the chip measures 2 mm by 5 mm.

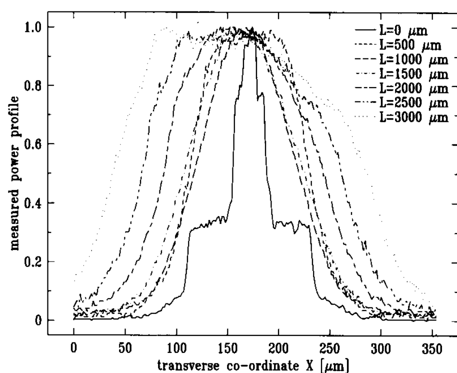

(a)

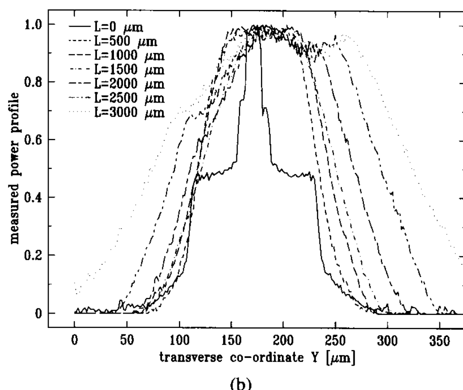

(b)

Fig. 11. Power density profiles for a number of propagation distances L, measured by a CCD camera. Profiles are presented in two orthogonal directions (labeled X and Y). Data is for the large aperture lens of Table II.

A flip chip mounted array of 36 LED's (2 × 18 at pitch 250 μm in the longitudinal and pitch 500 μm in the transversal direction), equipped with large aperture diffractive lenses is shown in Fig. 10. The chip size is about 2 mm × 5 mm.

V. Measurement Results

Results presented here will be focused on those component aspects of interest for the optical interconnect application, including beam characteristics, power throughput, cross talk

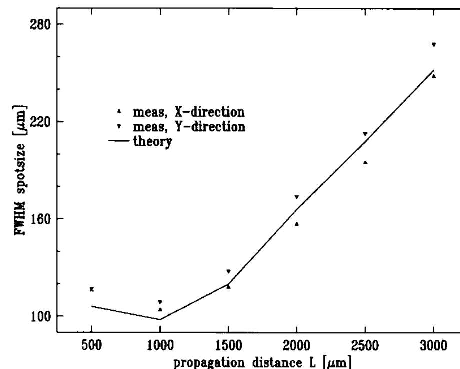

Fig. 12. Comparison of measured FWHM spotsizes (large aperture lens) and values obtained by ray tracing.

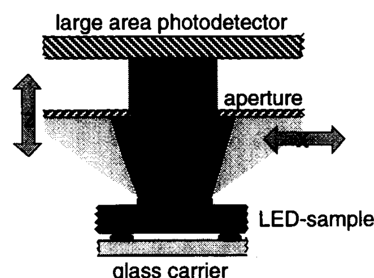

Fig. 13. Schematic drawing of experimental set-up for power throughput and cross talk evaluation.

and alignment properties. All measurements discussed here concern LED's with 6 μm mesa radius.

Spectral characteristics of the LED's are in good accordance with design goals: central wavelength 930 nm (designed for 925 nm) and full width half maximum optical spectral width 40 nm. Typical total emitted optical output powers are -16.8 dBm (small lens) and -11.4 dBm (large lens) for 10 mA drive current. Within one array the standard deviation in total optical power output amounts to 5% of its mean value.

To estimate beam shapes and full width half maximum spot sizes, light from the LED's was captured by a microscope objective and focused onto a CCD camera. Fig. 11 gives beam profiles in two orthogonal directions (labeled X and Y), for a number of propagation distances L. For a propagation distance of 2600 μm, the beam center was shifted 20 μm with respect to the optical axis, indicating a misalignment of ca. 1 μm between mesa's and diffractive lenses. Based on these graphs, FWHM spot sizes as a function of propagation distance were derived. These values are shown in Fig. 12, together with values obtained by ray tracing. Good agreement between experimental and modeled values can be seen, and the 400 μm spot size limit is met (assuring good power throughput–cross talk trade off).

Measurements of power throughput and cross talk were carried out using a set-up presented schematically in Fig. 13. Optical power incident through a number of apertures (250, 400, and 500 μm diameter) was assessed as a function of lateral (X) and longitudinal (Z) displacement. Table III(a)

TABLE III
FOCUSED POWER (a) RELATIVE TO TOTAL EMITTED OPTICAL POWER AND CROSS TALK, (b) RELATIVE TO FOCUSED POWER FOR THE TWO LENS TYPES

aperture radius	small lens	large lens
250 µm	-8.3 dB	-11.3 dB
400 µm	-6.8 dB	-9.7 dB
500 µm	-6.7 dB	-9.6 dB

(a)

aperture radius	small lens	large lens
250 µm	-13.7 dB	-13.0 dB
400 µm	-11.4 dB	-9.9 dB
500 µm	-10.0 dB	-8.7 dB

(b)

TABLE IV
ALIGNMENT TOLERANCE IN TRANSVERSE (a) AND LONGITUDINAL (b) DIRECTION

aperture radius	small lens	large lens
250 µm	55 µm	50 µm
400 µm	90 µm	106 µm
500 µm	80 µm	153 µm

(a)

aperture radius	small lens	large lens
250 µm	590 µm	327 µm
400 µm	1380 µm	1500 µm
500 µm	1500 µm	1360 µm

(b)

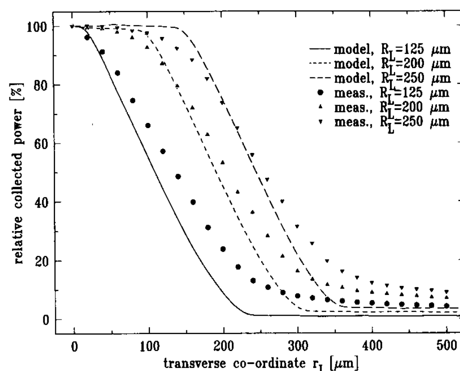

(a)

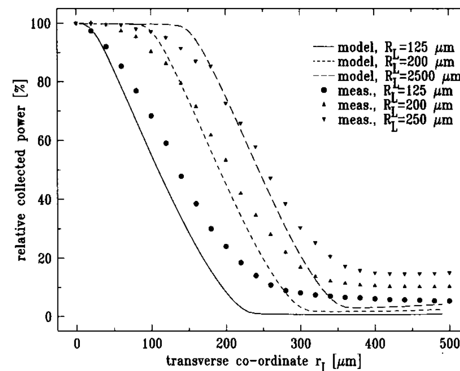

(b)

Fig. 14. Optical power focused through apertures (250, 400, and 500 μm diameter). Graph (a) first order lens, graph (b) hybrid lens.

gives values for power throughput for the three apertures (on axis $X = 0$ μm in the image plane $Z = 0$ μm) as a fraction of total emitted optical power. Corresponding nearest neighbor cross talk values, normalized to power throughput, are shown in Table III(b). It should be noted that in the case lensed detectors are used, the cross talk value will reduce considerably. Optical power focused on the detector as a function of lateral misalignment X (in the plane $Z =$ 0 μm), is given in Fig. 14 (values are normalized to on axis power throughput). Solid lines represent modeling results and experimental data are indicated with dots. Relatively good agreement between theory and experiment is established.

Tolerance towards lateral and longitudinal misalignments was evaluated using the following, somewhat arbitrary, criterion based on a combined power throughput and cross talk condition. In each case, the most limiting condition was used:

- maximum allowable drop in power throughput is 10%
- increase in cross talk limited to 1 dB.

Application of this criterion yields alignment tolerances of Table IV, showing that in all cases lateral misalignments of 50 μm can be tolerated while longitudinal alignments seem far less critical.

VI. CONCLUSION

LED-arrays for free space optical interconnect between adjacent computer boards were discussed. Monolithically integrated diffractive lenses were employed to collimate the LED-beams, which seems an attractive alternative to LED's with hybrid lenses. Design and fabrication issues were discussed, and a ray-tracing model was presented to predict performances (power density profiles, focusing properties, cross talk...) of the LED-lens combination. Devices were realized and experimental device characteristics are found in good accordance with both modeling results and application related constraints. Crucial parameters (power throughput, cross talk, alignment tolerances) are found in the right order of magnitude for proper operation of the board-to-board link. The LED-array with integrated diffractive lenses was therefore judged to be a good candidate (in terms of device fabrication complexity, mounting requirements and performances) for the optical interconnect application envisaged, and the construction of an optical interconnect demonstration making use of this type of board-to-board communication will be further pursued.

ACKNOWLEDGMENT

The authors gratefully acknowledge S. Verstuyft for his contribution to device processing and J. Blondelle wishes to thank the Belgian IWONL for financial support.

REFERENCES

[1] S. Kawai, "Free-space multistage optical interconnection networks using micro lens arrays," *J. Lightwave Technol.*, vol. 9, no. 12, pp. 1774–1779, Dec. 1991.

[2] O. Wada, S. Yamakoshi, M. Abe, Y. Nishitani, and T. Sakurai, "High radiance InGaAsP/InP lensed LED's for optical communication systems at 1.2–1.3 μm," *IEEE J. Quantum Electron.*, vol. QE-17, no. 2, pp. 174–178, Feb. 1981.

[3] B. Dhoedt, P. De Dobbelaere, and R. Baets, "Integration of Fresnel lenses with LED-arrays: Suitability for free space board to board interconnect," in *Tech. Dig. Gradient-Index Optical Systems Topical Meet.*, Santiago, Spain, Oct. 1992, pp. 60–63.

[4] B. Dhoedt, P. De Dobbelaere, J. Blondelle, R. Baets, P. Demeester, and P. Van Daele, "LED-arrays with integrated diffractive microlenses for free space optical interconnect," in *Tech. Dig. Microoptics Conf.*, Kawasaki, Japan, Oct. 1993, pp. 320–323.

[5] M. J. Goodwin, A. J. Mosely, M. G. Kearley, R. C. Morris, D. J. Groves-Kirkby, J. Thompson, R. C. Goodfellow, and I. Bennion, "Optoelectronic component arrays for optical interconnection of circuits and subsystems," *J. Lightwave Technol.*, vol. 9, no. 12, pp. 1639–1645, Dec. 1991.

[6] R. Magnusson and T. K. Gaylord, "Diffraction regimes of transmission gratings," *J. Opt. Soc. Am.*, vol. 68, no. 6, pp. 809–814, June 1978.

[7] E. Noponen, J. Turunen, and A. Vasara, "Electromagnetic theory and design of diffractive-lens arrays," *J. Opt. Soc. Am. A*, vol. 10, no. 3, pp. 434–443, Mar. 1993.

[8] T. K. Gaylord and M. G. Moharam, "Analysis and application of optical diffraction by gratings," *Proc. IEEE*, vol. 73, no. 5, pp. 894–937, May 1985.

[9] M. G. Moharam and T. K. Gaylord, "Three-dimensional vector coupled-wave analysis of planar-grating diffraction," *J. Opt. Soc. Am.*, vol. 73, no. 9, pp. 1105–1112, Sept. 1983.

Bart Dhoedt received the electrical engineering degree, specialization communication systems, from the University of Gent in 1990.

Since 1990, he has been employed as a research assistant by the Department of Information Techonology (INTEC) of the University of Gent and is currently working towards the Ph.D. degree in electrical engineering. His main research interests include diffractive optics, modeling and experimental assessment of optical and optoelectronic components for optical interconnects.

Peter De Dobbelaere received the degree of Electrotechnical Engineer at the Department of Information Technology of the University of Gent, Belgium, in 1989.

He has been working on the modeling and fabrication of diffractive optical elements. Currently he is involved in research in the fields of plasma processing and optoelectronic integration and packaging for guided wave and free space optical interconnections based on polymeric and III–V materials. He is working towards the Ph.D. degree at the University of Gent.

Johan Blondelle was born in Brugge, Belgium, in 1967. He received the degree in electrical engineering, specialization physics, from the University of Gent in 1992.

In August 1992 he joined the Department of Information Technology (former Laboratory of Electromagnetism and Acoustics) as a research assistant. In October 1992 he obtained a research scholarship from the Belgian IWONL (Institute for Encouragement of Scientific Research in Industry and Agriculture), for doing technology-oriented work focusing on LED's, detectors and integrated optics. He is currently working towards the Ph.D. degree.

Mr. Blondelle is a member of the Flemish Engineers Association.

Peter Van Daele received Ph.D. degree in electrical engineering in 1988 from the University of Gent.

From 1984 to 1988 he worked at the former Laboratory of Electromagnetism and Acoustics, now Department of Information Technology of the University of Gent in the field of integrated optoelectronic devices. Since 1988 he has been a permanent member of staff from IMEC at the Department of Information Technology of the University of Gent where he is responsible for the processing, fabrication and research on III–V optoelectronic and integrated photonic devices. He is involved or directly responsible for several RACE and ESPRIT-projects at the laboratory. Since April 1, 1993, he has been part time professor at the University of Gent. He is author or co-author of about 170 publications and presentations in international journals or at international conferences.

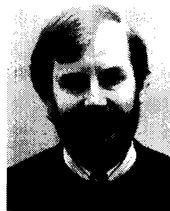

Piet Demeester (M'89) received the M.Sc. and Ph.D. degrees in electrical engineering from the University of Gent, in 1984 and 1988, respectively.

Since 1987 he has been employed by the Interuniversity Micro-Electronics Center (IMEC) and works in the Department of Information Technology (INTEC) at the University of Gent. He is coordinating the work on epitaxial growth and epitaxial lift-off for III–V optoelectronic devices and recently he also started research on modeling and simulation of broad-band communication networks. He is teaching digital signal processing as a part-time professor at the University of Gent.

Roel Baets (M'88), for a photograph and biography, see page 1064 of this issue.